STM and STS of Oxide Ultrathin Films

MR Castell, University of Oxford, Oxford, United Kingdom

Introduction

A typical ultrathin oxide film consists of a single monolayer of an oxide material on a crystalline metal support. In some circumstances, the film might consist of two or three monolayers, but generally these ultrathin films are no more than a nanometer in thickness and can be thought of as 2D materials.[1] Scanning tunneling microscopy (STM) is an excellent method for the study of these films because this technique allows surfaces to be imaged at very high magnifications.[2] To obtain atomic resolution images, STM requires the sample to be electrically conducting, free of surface contaminants, and flat on the atomic scale. Not only can STM reveal the structure of surfaces and thin films, it can also be used to study defects at the atomic level, such as atomic vacancies and impurities[3] or more extended structures such as domain boundaries where two ultrathin films of different crystallographic orientations meet. STM also enables very detailed investigation of amorphous oxide films.

Ultrathin oxide films are of interest in numerous applications where surface chemical reactions or surface atomic structure are critical.[4] A good example of this is the use of STM for the study of catalytically active oxides and oxide supports. Many common oxides such as MgO or Al_2O_3 are electrically insulating and are therefore not suitable for STM. However, if the oxides are grown in ultrathin film form on a conducting metal support, then the tunneling current of the STM can penetrate through the film, and atomic resolution images of the surface of the insulating film can be obtained. For example, STM has been used to image the dissociation of a single water molecule adsorbed on an ultrathin MgO (001) film supported by an Ag(001) substrate.[5] STM imaging of ultrathin films of Al_2O_3 is possible when grown on a NiAl(110) crystal.[6] Other catalysis-related STM studies of ultrathin oxide films involve imaging oxide encapsulated noble metal nanoparticles. This involves the so-called strong metal support interaction (SMSI). In this scenario, a catalytically active noble metal particle with a high surface energy, such as Pt, is supported on a metal oxide substrate with a relatively low surface energy, such as TiO_2. The total energy of the system can be reduced by covering the metal with a layer of oxide. If this system is at a temperature where diffusion can occur, then this often results in an ultrathin TiO_x film encapsulating the noble metal crystal. These oxide overlayers have been studied extensively using STM and often have complicated surface structures.[7]

There is also interest in the formation of ultrathin oxide films in the context of the study of the early stages of corrosion. For example, an STM operating in an electrochemical cell has been used to study the formation of ultrathin oxide films of Cu_2O on a polycrystalline sample, allowing the investigation of how grain boundaries are preferentially affected during corrosion.[8] Oxide thin film studies related to the fields of microelectronics[9] and spintronics[10] are also regularly carried out using scanning tunneling spectroscopy (STS) and STM. These examples demonstrate the versatility of the use of STM and STS for the study of oxide ultrathin films. In the following sections, a variety of different types of ultrathin oxide films are discussed, and their study using STM are presented.

STM of Simple Oxide Films

The reason that ultrathin oxide films can form as a single monolayer is the same reason that oil spreads out on the surface of water, namely due to a minimization of surface and interface energies. The surface energy of oxides tends to be significantly lower than that of their pure constituent elements, so that when a material is exposed to oxygen, an ultrathin oxide overlayer forms. This can be illustrated by considering the structure of a pure Ni(001) crystal that is exposed to oxygen, where the oxidation process occurs through random interactions with the surface until a NiO(001) overlayer is formed. Studies of this process were some of the earliest STM investigations of ultrathin oxide films.[11] However, Ni is not a good substrate for the growth of NiO because of the large difference in the lattice constants of Ni (0.352 nm) and NiO (0.417 nm). A better substrate is the Ag(001) crystal surface because Ag has a more closely matched lattice constant of 0.409 nm, resulting in only a 2% mismatch strain. A NiO ultrathin film can be grown on Ag(001) by evaporating a small amount of Ni on the substrate and then annealing

Encyclopedia of Interfacial Chemistry, 2018, 332–337

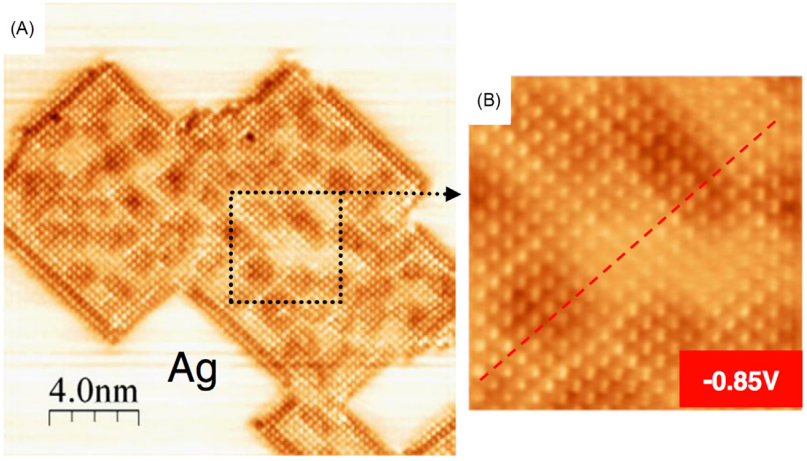

Fig. 1 (A) STM image of an Ag(001) substrate that appears light and has a dark NiO(001) island embedded in it (image width 20 nm). (B) *Close-up* view of the *dotted square* section in (A) showing atomic corrugations (image width 5 nm). Sample bias −0.85 V, tunneling current 0.5 nA. Image adapted from Steurer, W.; Surnev, S.; Fortunelli, A.; Netzer, F. P. Scanning Tunneling Microscopy Imaging of NiO(100)(1 × 1) Islands Embedded in Ag(100). *Surf. Sci.* **2012**, *606*, 803–807.

it in an oxidizing environment. The interaction of the evolving NiO(001) film with the Ag(001) substrate allows the oxide film to wet the substrate and grow as an epitaxial 2D material, as shown in Fig. 1.[12] In this STM image, the NiO(001) film is, to a significant extent, similar to the top layer of a bulk termination of a NiO(001) crystal.[13] In other words, for this example, the main function of the substrate is to act as a support with a low interface energy, but the support itself does not change the inherent structure of the film compared with the bulk. In the next section, examples are shown where the substrate has a strong influence on the structure of the film.

STM of Oxide Films with Unique Structures

In general, for oxide ultrathin films, the interaction of the film with the substrate is a critical element in determining the atomic and electronic structure of the film. This is in contrast to other 2D materials such as graphene that are stable as freestanding monolayers and where there is only a weak interaction with the support. For example, a freestanding monolayer of Ti_2O_3 is not stable, but through the interaction with an Au(111) surface,[14] it forms a well-ordered overlayer, as shown in the STM image in Fig. 2A. The atomic arrangement of this structure is shown in Fig. 2B. It is known as a honeycomb 2×2 lattice as the unit cell of the honeycomb is twice the size of the Au(111) surface unit cell. There is an epitaxial relationship of the honeycomb lattice with the Au(111) surface, meaning that the structure of the honeycomb lattice is in great part determined by the crystallography of the Au(111) substrate. Every Ti atom is located at a threefold hollow site on the Au(111) surface. The electronegativity of the Au substrate also plays a part in stabilizing this ultrathin film structure.[15] One might therefore expect to see other instances of this honeycomb structure on electronegative noble metal supports, and indeed this is the case. The STM image in Fig. 2C is of honeycomb Ti_2O_3 on Pt(111),[16] and the image in Fig. 2D is of honeycomb V_2O_3 on Pd(111).[17] The honeycomb lattice has also been found to exist in the Nb_2O_3 on Au(111) system.

As can be seen from the images in Fig. 2C and D, the oxide ultrathin film is not perfect, but contains defects. These are readily imaged using STM and can be of various forms. For example, simple O or Ti/V vacancies can be imaged, as can defective arrangements of the honeycomb lattice itself, where the usual 6-member rings are replaced by 5-member or 7-member rings. Two Stone-Wales defects can be seen in Fig. 2D, which are groupings of two 7-member rings and two 5-member rings. Similar defects are also seen in the more familiar graphene hexagonal lattice. Where the epitaxial domains of the honeycomb lattice are not perfectly aligned, there are also extended domain boundaries, as can be seen in Fig. 2C. Four, five, seven, and eight-membered rings are present in these boundary structures. These effects are due to epitaxy, but in the next section, ultrathin oxide films that only have a weak crystallographic relationship with the substrate are shown, and this gives rise to so-called moiré patterns.

STM of Oxide Films with a Moiré Pattern

Moiré patterns appear in the structure of ultrathin oxide films when the crystallographic periodicities of the substrate and the oxide film are slightly different and/or rotated with respect to each other. A nice example of this is the FeO overlayer on a Pt(111) surface, as shown in the STM image in Fig. 3A, next to the atomic structural model shown in Fig. 3B.[18] The periodicity of the FeO film is around 10% greater than that of the Pt(111) substrate, which means that the overlayer and the substrate cannot form a simple

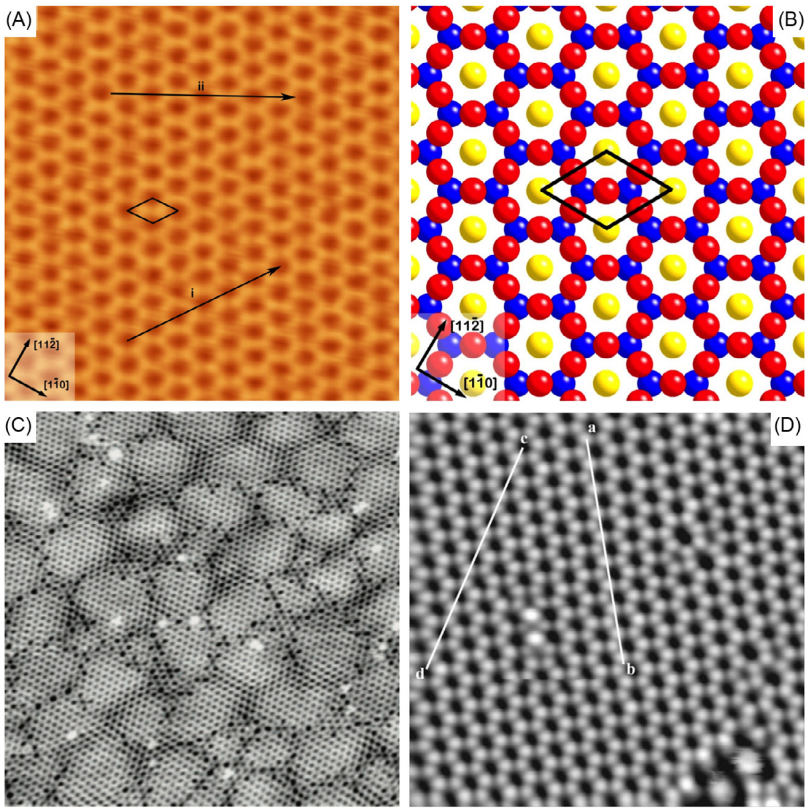

Fig. 2 Honeycomb overlayers on noble metal (111) substrates. (A) STM image of Ti_2O_3 on Au(111) (Image adapted from Wu, C.; Marshall, M. S. J.; Castell, M. R. Surface Structures of Ultrathin TiOx Films on Au(111). *J. Phys. Chem. C* **2011**, *115*, 8643–8652). Image width 8.5 nm, sample bias 0.98 V, and tunneling current 0.2 nA. (B) Atomic model of the 2×2 Ti_2O_3 honeycomb overlayer structure. The Au substrate atoms are *gold*, the hollow site titanium atoms are *blue*, and the top layer of oxygen atoms is *red*. (C) STM image of Ti_2O_3 on Pt(111). Image width 30 nm, sample bias 1 V, and tunneling current 1.0 nA (Image adapted from Sedona, F.; Rizzi, G. A.; Agnoli, S., et al. Ultrathin TiOx Films on Pt(111): A LEED, XPS, and STM Investigation. *J. Phys. Chem. B* **2005**, *109*, 24411–24426). (D) STM image of V_2O_3 on Pd(111). Image width 8 nm, sample bias 0.05 V, and tunneling current 1.0 nA (Image adapted from Surnev, S.; Vitali, L.; Ramsey, M. G., et al. Growth and Structure of Ultrathin Vanadium Oxide Layers on Pd(111). *Phys. Rev. B* **2000**, *61*, 13945–13954).

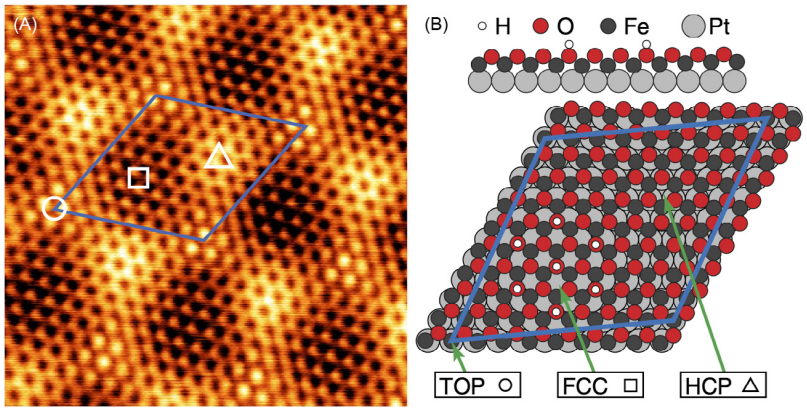

Fig. 3 (A) STM image of an FeO monolayer moiré film on a Pt(111) surface. Image width 6.5 nm, sample bias 0.065 V, and tunneling current 3 nA. The on top sites are indicated with a *circle*, the fcc sites with a *square*, and the hcp sites with a *triangle*. The structural model is shown in (B). Images taken from Merte, L. R.; Bechstein, R.; Peng, G. W., et al. Water Clustering on Nanostructured Iron Oxide Films. Nat. Commun. **2014**, *5*, 4193.

epitaxial relationship, as was the case for the honeycomb films discussed previously. The Fe atoms are situated in a variety of locations on the Pt(111) surface including hollow sites (both hcp and fcc), bridge sites, and on top sites. How the Fe atoms are situated with respect to the Pt(111) substrate has both geometric and electronic effects. For example, an Fe atom on an on top site will be in a geometrically higher position than the one situated in a hollow site. These variations give rise to the undulating change in brightness across the image. The fine scale periodicity in the image is due to the Fe ions. This is because the local density of states contribution of the Fe ions has a dominant effect over the more prominently positioned O ions. There are numerous other systems where moiré oxide films have been imaged by STM, for example CoO on Pt(111),[19] or TiO_x on Pd(111).[20]

STM of Oxide Ultrathin Films with Amorphous Structures

Most ultrathin oxide films have a crystalline structure. This is also the case for $SiO_{2.5}$ monolayers on metals with high oxygen adsorption energies, but on noble metals silica tends to grow as a bilayer film with composition SiO_2.[21] This bilayer can exist in a crystalline or in an amorphous state, as shown in the STM images in Fig. 4.[22] In this example, a SiO_2 bilayer was grown on a Ru(0001) surface. The crystalline phase on the left side of the images in Fig. 4 is dominated by hexagonal rings, but on the right side, there are rings that vary from 4 to 9 Si atoms. The boundary between the crystalline and amorphous phase can be clearly seen. Although the rings are of different sizes, the atoms are all coordinated in the same way, so that the amorphous phase also has SiO_2 stoichiometry. These two-dimensional amorphous films turn out to have meaningful structural relationships with three-dimensional amorphous structures. This is important because it is possible to visualize atomic positions in 2D films, allowing important structural insights to be gleaned, while it is not possible to map amorphous solids at atomic resolution.

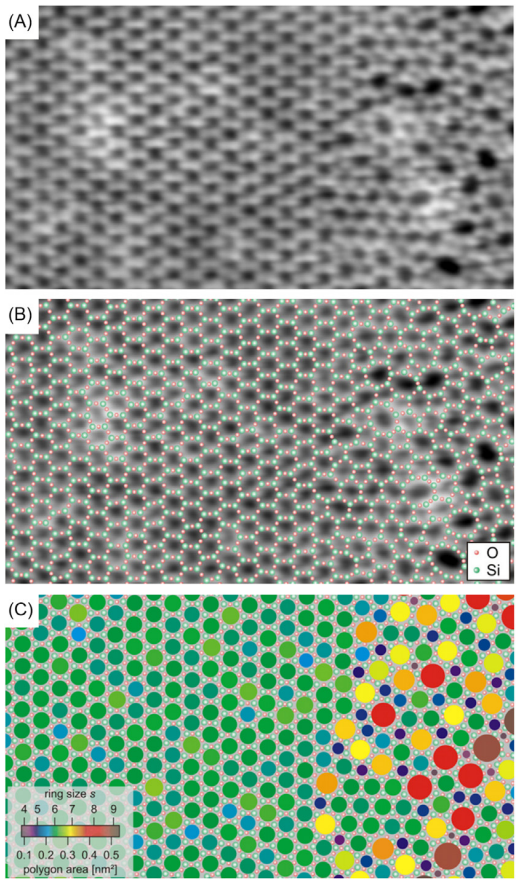

Fig. 4 (A) STM image of a silica bilayer film on Ru(0001) with both crystalline and amorphous regions. (B) The image in (A) with the atomic locations of the Si and O atoms superimposed. (C) Image analysis of the ring sizes. The crystalline hexagonal rings dominate the *left* side of the image, while the rings in the amorphous phase vary from 4 to 9. Image width 12.3 nm, sample bias 2 V, and tunneling current 0.1 nA. Images taken from Lichtenstein, L.; Heyde, M.; Freund, H. J. Crystalline-Vitreous Interface in Two Dimensional Silica. Phys. Rev. Lett. **2012**, *109*, 106101.

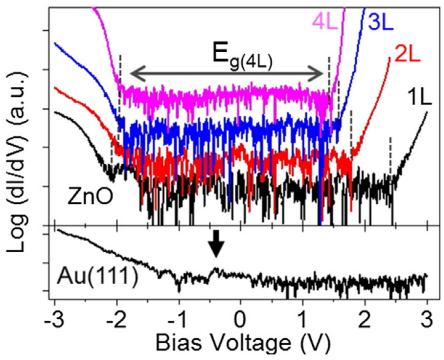

Fig. 5 Differential tunneling conductance spectra demonstrating the bandgap narrowing for ZnO layers of thicknesses ranging from a single monolayer (1 L) to four monolayers (4 L). The *lower* spectrum is of the bare Au(111) support, with the Au surface state *arrowed*. Figure taken from Lee, J.; Sorescu, D. C.; Deng, X. Y. Tunable Lattice Constant and Band Gap of Single- and Few-Layer ZnO. *J. Phys. Chem. Lett.* **2016**, *7*, 1335–1340.

STS of Oxide Ultrathin Films

STS involves placing the STM tip above a fixed point on the sample and varying the voltage between the tip and the sample. The change in the tunneling current as a function of the change in the voltage is a measure of the local density of states of the sample. This allows high-energy resolution electronic structure spectroscopy with atomic precision to be carried out in both the filled and empty states. The energy range generally does not extend beyond ± 3 V around the Fermi energy. Most high-quality STS studies on oxides have been conducted to study their low temperature superconducting behavior. For many of these studies, the thin films are thick enough to be bulk analogues. There are, however, some interesting STS investigations of oxide ultrathin films on metal supports. A good example is a study of ultrathin ZnO(0001) films grown on Au(111) substrates.[23] In this experiment, ZnO films of thicknesses varying from 1 to 4 monolayers were investigated. The bandgap of the films was shown to decrease from 4.5 eV for a single monolayer to 3.4 eV for a film with a four-monolayer thickness. The tunneling spectra are shown in Fig. 5. The bandgap at four monolayers is close to that of bulk ZnO, demonstrating that at least four monolayers of ZnO are required before the film becomes bulk-like. This STS data set only uses the measurement of the bandgap for the ultrathin film; however, other electronic states are also detectable, such as the Au surface state that is also shown in Fig. 5.

Conclusion

This chapter has covered a number of uses of STM and STS for the study of oxide ultrathin films. It has not attempted to be an exhaustive review of the literature, but rather, has used pertinent examples to illustrate the broad range of application of the techniques. There are further topics, not covered here, such as using STM for in situ ultrathin film growth studies and tracking defect diffusion. Another related important use of STM, especially in relation to catalysis, is to study the adsorption behavior and dynamics of molecules and adsorbed atoms on oxide ultrathin films. There is also an established field of research related to metal island growth on oxide films.[2] Here STM can provide information related to the nucleation, size, shape, distribution, and ripening behavior of the metal nanoclusters and islands. A further emerging research area relates to the study of the unusual behavior of ultrathin ternary oxide films, such as $BaTiO_3$. STM studies of this system have shown that in ultrathin film form quasicrystalline order[24] or labyrinth phases[15] can be generated.

See also: Characterization of ultrathin oxide films by LEEM/PEEM; Surface Science Approach to Catalyst Preparation Using Thin Oxide Films as Substrates; Ultrathin Oxide Films on Ferromagnetic Metallic Substrates; Ultrathin Transition Metal Oxide Films.

References

1. Netzer, F. P.; Fortunelli, A. *Eds.; Oxide Materials at the Two-Dimensional Limit*, Springer: Berlin, 2016.
2. Nilius, N. Properties of Oxide Thin Films and their Adsorption Behavior Studied by Scanning Tunneling Microscopy and Conductance Spectroscopy. *Surf. Sci. Rep.* **2009,** *64,* 595–659.
3. Marshall, M. S. J.; Castell, M. R. Scanning Tunnelling Microscopy of Epitaxial Nanostructures. *Chem. Soc. Rev.* **2014,** *43,* 2226–2239.
4. Pacchioni, G., Valeri, S., Eds. *Oxide Ultrathin Films: Science and Technology*, Wiley: New York, 2011.
5. Shin, H.-J.; Jung, J.; Motobayashi, K.; et al. State-Selective Dissociation of a Single Water Molecule on an Ultrathin MgO Film. *Nat. Mater.* **2010,** *9,* 442–447.
6. Heinke, L.; Lichtenstein, L.; Simon, G. H.; et al. Structure and Electronic Properties of Step Edges in the Aluminum Oxide Film on NiAl(110). *Phys. Rev. B* **2010,** *82*, 075430.

7. Dulub, O.; Hebenstreit, W.; Diebold, U. Imaging Cluster Surfaces with Atomic Resolution: The Strong Metal-Support Interaction State of Pt Supported on TiO_2(110). *Phys. Rev. Lett.* **2000,** *84,* 3646–3649.
8. Chen, H.; Bettayeb, M.; Maurice, V.; et al. Local Passivation of Metals at Grain Boundaries: In Situ Scanning Tunneling Microscopy Study on Copper. *Corros. Sci.* **2016,** *111,* 659–666.
9. Thamankar, R.; Raghavan, N.; Molina, J.; et al. Single Vacancy Defect Spectroscopy on HfO_2 Using Random Telegraph Noise Signals from Scanning Tunneling Microscopy. *J. Appl. Phys.* **2016,** *119*, 084304.
10. Parkinson, G. S. Iron Oxide Surfaces. *Surf. Sci. Rep.* **2016,** *71,* 272–365.
11. Baumer, M.; Cappus, D.; Kuhlenbeck, H.; et al. The Structure of Thin NiO(100) Films Grown on Ni(100) as Determined by Low-Energy-Electron Diffraction and Scanning Tunneling Microscopy. *Surf. Sci.* **1991,** *253,* 116–128.
12. Steurer, W.; Surnev, S.; Fortunelli, A.; Netzer, F. P. Scanning Tunneling Microscopy Imaging of NiO(100)(1×1) Islands Embedded in Ag(100). *Surf. Sci.* **2012,** *606,* 803–807.
13. Castell, M. R.; Wincott, P. L.; Condon, N. G.; et al. Atomic-Resolution STM of a System with Strongly Correlated Electrons: NiO(001) Surface Structure and Defect Sites. *Phys. Rev. B* **1997,** *55,* 7859–7863.
14. Wu, C.; Marshall, M. S. J.; Castell, M. R. Surface Structures of Ultrathin TiO_x Films on Au(111). *J. Phys. Chem. C* **2011,** *115,* 8643–8652.
15. Wu, C.; Castell, M. R.; Goniakowski, J.; Noguera, C. Stoichiometry Engineering of Ternary Oxide Ultrathin Films: $BaxTi_2O_3$ on Au(111). *Phys. Rev. B* **2015,** *91,* 155424.
16. Sedona, F.; Rizzi, G. A.; Agnoli, S.; et al. Ultrathin TiO_x Films on Pt(111): A LEED, XPS, and STM Investigation. *J. Phys. Chem. B* **2005,** *109,* 24411–24426.
17. Surnev, S.; Vitali, L.; Ramsey, M. G.; et al. Growth and Structure of Ultrathin Vanadium Oxide Layers on Pd(111). *Phys. Rev. B* **2000,** *61,* 13945–13954.
18. Merte, L. R.; Bechstein, R.; Peng, G. W.; et al. Water Clustering on Nanostructured Iron Oxide Films. *Nat. Commun.* **2014,** *5,* 4193.
19. De Santis, M.; Buchsbaum, A.; Varga, P.; Schmid, M. Growth of Ultrathin Cobalt Oxide Films on Pt(111). *Phys. Rev. B* **2011,** *84,* 125430.
20. Bennett, R. A.; Pang, C. L.; Perkins, N.; et al. Surface Structures in the SMSI State; Pd on (1×2) Reconstructed TiO_2(110). *J. Phys. Chem. B* **2002,** *106,* 4688–4696.
21. Shaikhutdinov, S.; Freund, H. J. Ultrathin Silica Films on Metals: The Long and Winding Road to Understanding the Atomic Structure. *Adv. Mater.* **2013,** *25,* 49–67.
22. Lichtenstein, L.; Heyde, M.; Freund, H. J. Crystalline-Vitreous Interface in Two Dimensional Silica. *Phys. Rev. Lett.* **2012,** *109,* 106101.
23. Lee, J.; Sorescu, D. C.; Deng, X. Y. Tunable Lattice Constant and Band Gap of Single- and Few-Layer ZnO. *J. Phys. Chem. Lett.* **2016,** *7,* 1335–1340.
24. Forster, S.; Meinel, K.; Hammer, R.; Trautmann, M.; Widdra, W. Quasicrystalline Structure Formation in a Classical Crystalline Thin-film System. *Nature* **2013,** *502,* 215.